BEFIB2012 – Fibre reinforced concrete
Joaquim Barros et al. (Eds)
UM, Guimarães, 2012

A DESIGN MODEL FOR FIBRE REINFORCED CONCRETE BENDING ELEMENTS WITH LONGITUDINAL PRE-STRESSED STEEL AND FRP BARS

M. Taheri[*] , J.A.O. Barros[†] and H. Salehian[**]

[*] ISISE, Dep. Civil Eng., School Eng., University of Minho
Campus de Azurém 4800-058 Guimarães, Portugal
e-mail: taheri@civil.uminho.pt, web page: www.isise.net

[†] ISISE, Dep. Civil Eng., School Eng., University of Minho
Campus de Azurém 4800-058 Guimarães, Portugal
e-mail: barros@civil.uminho.pt, web page: www.isise.net

[**] ISISE, Dep. Civil Eng., School Eng., University of Minho
Campus de Azurém 4800-058 Guimarães, Portugal
e-mail: salehian@civil.uminho.pt, web page: www.isise.net

Keywords: Tensile-strain softening, tensile-strain hardening, pre-stressing, fibre reinforced concrete, moment-curvature response, load-deflection response.

Summary: *A close form solution to calculate the moment-curvature and load-deflection response of strain-softening and strain-hardening fibre reinforced concrete (FRC) elements failing in bending and reinforced longitudinally with pre-stressed steel and fibre reinforce polymer (FRP) bars is presented. This hybrid reinforcement is used for the development of high durable pre-fabricated and cost competitive beams. Pre-stressed FRP bars are applied with the minimum concrete cover, in order to take into account the benefits derived from the relatively high tensile strength of these bars and their immunity to corrosion. Pre-stressed steel bars, with a larger concrete cover have the purpose of providing the necessary ductility and assure the resistance of the beam in case of a fire occurrence. To replace completely the steel stirrups, a high performance fibre reinforced concrete is used. The predictive performance of the model is assessed by taking advantage of FEMIX, a FEM-based computer program. The model is finally utilized in a parametric study in order to evaluate the impact of post-cracking performance of FRC and applied pre-stress percentage on structural performance of FRC beams.*

1   INTRODUCTION

The inherent weakness of concrete in tension is being remedy by applying steel bars in the execution of reinforced concrete (RC) structures. However, penetration of corrosives agents through cracks formed since concrete early age, and through the porous nature of the concrete micro-structure, affects negatively the reinforcement performance provided by steel bars, due to the corrosion of these bars and the consequent splitting of surrounding concrete. To avoid corrosion related problems, mainly in aggressive environments, the use of fibre reinforced polymer (FRP) bars has been investigated [1] as an alternative reinforcement system to conventional steel bars.

When compared to steel, the FRPs have higher resistance to corrosion. Due to economic reasons, glass fibre reinforced polymer (GFRP) bars are the most used FRPs for the reinforcement of concrete structures. However, due to the relative low modulus of elasticity of GFRP bars, for the same

reinforcement ratio, FRP reinforced elements present higher deflection and strains, and larger crack widths than in the case where steel bars are used [2]. Furthermore, the high initial costs, the lack of ductility and the still reduced number of reliable design formulations for the prediction of the behaviour of FRP-RC elements [3, 4], are contributing for the relative low use of this reinforcement in concrete technology.

These drawbacks can be overcome by combining FRP and steel bars [5], in which FRP bars are positioned near the outer surface of the tensile zone with the minimum concrete cover that assures the necessary FRP-concrete bond requisites, while steel bars are placed with a concrete cover thickness that provides high resistance to corrosion attack. The benefits of such hybrid reinforcement can be explored to decrease flexural deflections and maximum crack width [2, 5]. If pre-stressed steel and FRP bars are utilized, smaller distance and width of cracks, as well as higher steel yielding loads can be obtained [6]. Steel stirrups are the reinforcement elements more prone to corrosion since they are the closest ones to the external surface of the structural elements. Therefore, to replace steel stirrups, fibre reinforced cement composites (FRC) is recommended [7] since this material can also improve the bond behaviour of longitudinal tensile pre-stressed bars due to the reinforcement mechanisms provided by discrete fibres that offer resistance to the coalescence of micro- into macro-cracks. Depending on the type and volume of used fibres, and characteristics of cement based material, the FRC can present a strain softening (SS) or a strain hardening (SH) tensile behaviour [8]. The SSFRC has a post peak strength (σ_{cst}) that is smaller than the stress at crack initiation (σ_{cr}), while a SHFRC develop a post-cracking strength that is higher than σ_{cr}.

In the present paper the flexural behaviour of a FRC member reinforced longitudinally by pre-stressed steel and FRP bars was investigated. Assuming simplified stress-strain responses for FRC in tension and compression, as well as for tensile steel and FRP bars, a closed form solution was developed to determine the moment versus curvature relationship ($M - \chi$). By using the $M - \chi$ curve, the load versus deflection response of a statically determinate hybrid FRC beam of rectangular section can be determined. The accuracy of the proposed model was appraised by comparing the results with those obtained from a FEM based computer program capable of simulating the nonlinear behaviour of the constituent materials [9]. The model was finally utilized in a parametric study to investigate the effect of FRC post cracking performance and the applied pre-stress percentage on the moment-curvature and load-deflection response of beams that was assumed failing in bending.

2   Numerical strategy for the evaluation of the moment-curvature and force-deflection of FRC-hybrid pre-stressed beams

The model was developed for a rectangular cross section of width *b* and depth *d* (Fig. 1) that can be reinforced with steel and FRP bars, being $\rho_s = A_s / (bd_s)$ and $\rho_f = A_f / (bd_f)$ the reinforcement ratio of steel and FRP bars, respectively, where A_s and A_f are the cross sectional area of steel and FRP bars, and $d_s = d - C_s$ and $d_f = d - C_f$ are the internal arms of steel and FRP bars, respectively, being C_s and C_f the concrete cover for the steel and FRP bars.
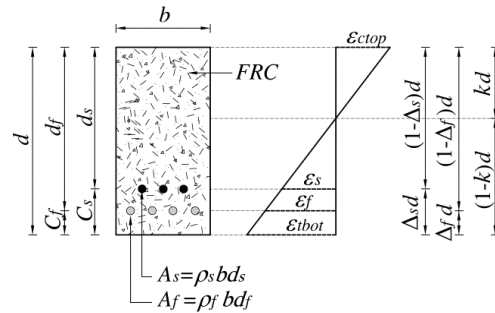
Figure 1: Concept of FRC-hybrid reinforcing system, and variables involved in the analytical model.

2.1 Constitutive laws for the intervening materials

Stress-strain response in tension and compression considered for FRC is represented in Fig. 2a and 2b, respectively [10]. The tensile behaviour of FRC is started by an elastic range defined by the elasticity modulus E, followed by a post-cracking modulus (E_{cr}) that can be obtained by using a post-crack modulus parameter (η). By setting η to either a negative or a positive value, the same model can be used to simulate SS- or SH-FRCs, respectively. At the third region of the tensile response, tensile stress (σ_{cst}) remains constant up to the ultimate tensile strain (ε_{tu}) that is a multiple of the cracking strain, e.g. $\varepsilon_{tu} = \beta_{tu} \, \varepsilon_{cr}$. Introducing the concept of residual strength parameter, μ, the σ_{cst} can be defined as function of the stress at crack initiation, $\sigma_{cst} = \mu \sigma_{cr}$.
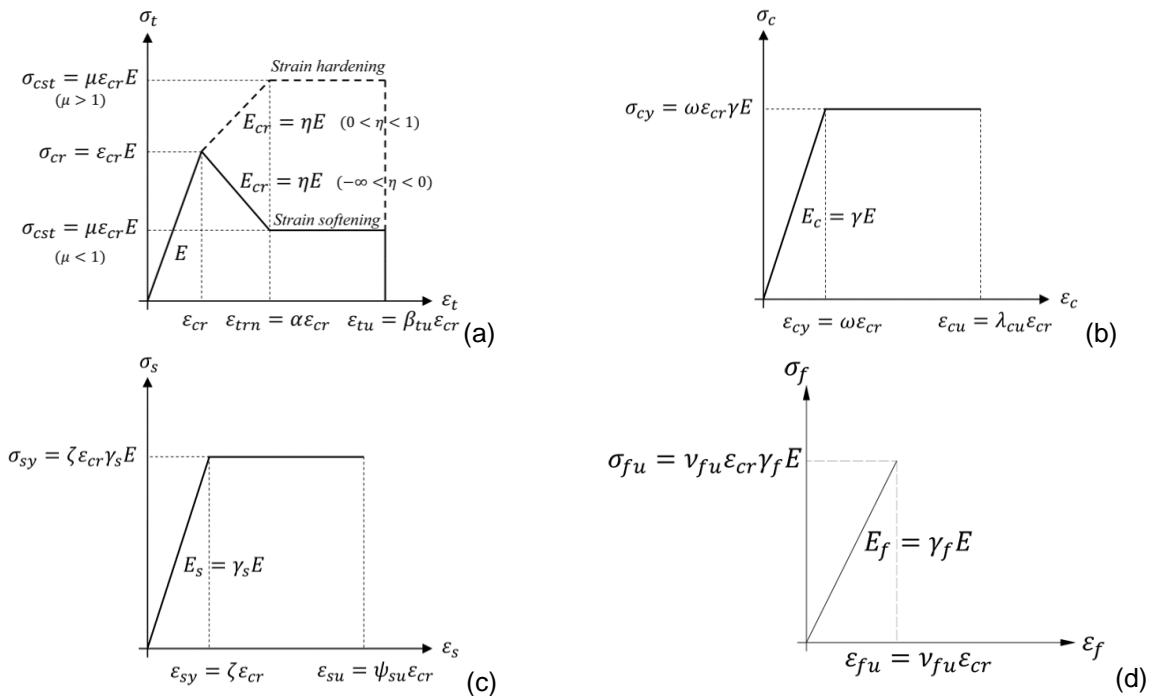

Figure 2: Stress-strain diagrams of : a) SS- and SH-FRC in tension [10]; b) FRC in compression [10]; c) tensile steel bars; d) tensile FRP bars

3

Compressive response of FRC is assumed linear-elastic in the first phase that terminates at a "pseudo-yield" point $\left(\varepsilon_{cy}, \sigma_{cy}\right)$, and it is followed by a phase of constant compressive "yield" stress, σ_{cy}, until the ultimate compressive strain, ε_{cu}. Young's Modulus in compression (E_c), can be determined from E by using a normalized compressive stiffness factor (γ): $E_c = \gamma E$. In this model ω is the normalized compressive "yield" strain, and β_{tu} and λ_{cu} are the normalized ultimate tensile and compressive strain, respectively. The transition between the tensile softening/stiffening to the constant residual tensile strength phase is defined by the α parameter, $\varepsilon_{tm} = \alpha \varepsilon_{cr}$.

A bilinear stress-strain diagram is assumed for tensile steel bars as depicted in Fig. 2c, in which the first linear elastic branch ends at the yield strain $\left(\varepsilon_{sy} = \zeta \varepsilon_{cr}\right)$, followed by a perfectly plastic branch ($\sigma_{sy} = E_s \varepsilon_{sy}$) up to attain the ultimate tensile strain ($\varepsilon_{su} = \psi_{su} \varepsilon_{cr}$), after which the steel tensile strength capacity is assumed null. The steel modulus of elasticity ($E_s = \gamma_s E$) is defined from the FRC tensile modulus of elasticity (E) by using the steel stiffness factor (γ_s).

Fig. 2d shows the linear-elastic stress-strain diagram considered for FRP bars in tension that ends at the ultimate tensile strain ($\varepsilon_{fu} = v_{fu} \varepsilon_{cr}$) of the FRP bar. Using the FRP tensile stiffness factor (γ_f), the modulus of elasticity of the FRP is defined from E ($E_f = \gamma_f E$).

2.2 Closed-formulation to determine the moment-curvature response

The tensile and compressive stress relationships of the cross section components can be normalized by the FRC stress at crack initiation, σ_{cr} ($= E \varepsilon_{cr}$), according to the following equations:

$$\frac{\sigma_t(\beta)}{E \varepsilon_{cr}} = \begin{cases} \beta & 0 < \beta \leq 1 \\ 1 + \eta(\beta - 1) & 1 < \beta \leq \alpha \\ \mu & \alpha < \beta \leq \beta_{tu} \\ 0 & \beta > \beta_{tu} \end{cases} \tag{1}$$

$$\frac{\sigma_c(\lambda)}{E \varepsilon_{cr}} = \begin{cases} \gamma \lambda & 0 < \lambda \leq \omega \\ \gamma \omega & \omega < \lambda \leq \lambda_{cu} \\ 0 & \lambda > \lambda_{cu} \end{cases} \tag{2}$$

$$\frac{\sigma_s(\psi)}{E \varepsilon_{cr}} = \begin{cases} \gamma_s \psi & 0 < \psi \leq \zeta \\ \gamma_s \zeta & \zeta < \psi \leq \psi_{su} \\ 0 & \psi > \psi_{su} \end{cases} \tag{3}$$

$$\frac{\sigma_f(v)}{E \varepsilon_{cr}} = \begin{cases} \gamma_f v & 0 < v \leq v_{fu} \\ 0 & v > v_{fu} \end{cases} \tag{4}$$

The normalized compressive strain at the concrete top fibre (λ), and the normalized tensile strain of the steel (ψ) and FRP (v) can be linearly correlated to the normalized tensile strain at the concrete bottom fibre (β):

$$\lambda = k \beta / (1 - k) \; ; \; \psi = (1 - k - \Delta_s) \beta / (1 - k) \; ; \; v = (1 - k - \Delta_f) \beta / (1 - k) \tag{5}$$

where k, Δ_s and Δ_f are the neutral axis depth ratio, and the normalized central distance of steel and FRP bars from tensile face of section, respectively (Fig. 1). To apply a certain pre-stress level to both steel and FRP bars, two independent initial tensile strains are considered, designated by steel pre-

stressing strain, ε_s^{pr}, and FRP pre-stressing strain, ε_f^{pr}, respectively. The pre-stress level for the steel and FRP bars is defined as the ratio between ε_s^{pr} and the steel tensile yield strain (ε_{sy}), and the ratio between ε_f^{pr} and the FRP ultimate tensile strain (ε_{fu}), respectively. Assuming the variation of pre-stress levels in the range [0-1] (for FRP bars the pre-stress level is, in general, limited to 0.6 [2]), pre-stressed strains are restricted to the linear elastic region of steel and FRP tensile stress-strain response (Figs. 2c and 2d). Therefore, the pre-stress loads for the steel (F_s^{pr}) and FRP (F_f^{pr}) are obtained from the following equations:

$$F_s^{pr} = \varepsilon_s^{pr} \gamma_s E \rho_s b d_s \tag{6}$$

$$F_f^{pr} = \varepsilon_f^{pr} \gamma_f E \rho_f b d_f \tag{7}$$

Regarding to the depth of the neutral axis (kd), the bending moments corresponding to pre-stress loads are calculated by the following equations:

$$M_s^{pr} = F_s^{pr} (1 - k - \Delta_s) d \tag{8}$$

$$M_f^{pr} = F_f^{pr} (1 - k - \Delta_f) d \tag{9}$$

To calculate the moment-curvature ($M - \chi$) diagram, it is assumed that a plane section remains plane after bending, and shear deformation of the section can be ignored. A gradual increment is applied to the normalized tensile strain at the concrete bottom fibre (β), and corresponding values of λ, ψ, and ν are obtained from Eqs. (5).

Due to the specificities of the constitutive laws of the intervening materials, nine strain configurations need to be considered [11]. For each strain configuration the value of k parameter can be obtained by the equations presented in Table 1 [11]. With respect to the k_i (the neutral axis depth in the *ith* stage) the normalized resisting moment ($M_i' = M_i / M_{cr}$) and the corresponding curvature ($\chi_i' = \chi_i / \chi_{cr}$) are obtained from equations in Table 2 [11], where M_{cr} and χ_{cr} are the cracking moment and the corresponding curvature, respectively:

$$M_{cr} = bd^2 (E \varepsilon_{cr}) / 6 \tag{10}$$

$$\chi_{cr} = 2\varepsilon_{cr} / d \tag{11}$$

2.3 Model to estimate the force-deflection relationship

The force-deflection response of a statically determinate beam failing in bending is determined by the algorithm schematically represented in Figure 3. According to this approach, for successive χ_i of the $M - \chi$ relationship of the beam's mid-span cross section the corresponding M_i is read, and the total applied load P_i is determined by equilibrium of the beam, as well as the beam bending diagram M_i. Decomposing the beam in small segments, the bending moment in a generic cross section at a distance x can be determined, $M_i(x)$, and from the $M - \chi$ relationship of this cross-section, the corresponding flexural stiffness $EI_i(x)$ is obtained, as well as the bending moment in this section for the base system corresponding to the evaluation of the deflection at the beam mid-span, $\bar{M}(x)$.

Table 1 - Equations for the evaluation of the depth of the neutral axis parameter, k, for stage i [11].

i	k
1	$k_1 = \begin{cases} \dfrac{2B_s(1-\Delta_s) + 2B_f(1-\Delta_f) + 1 + \left(\dfrac{2}{\beta}\right)F_{pr}}{2\sqrt{D_1}} & \text{for } \gamma = 1 \\[4mm] \dfrac{-(1+B_s+B_f+(1/\beta)F_{pr}) + \sqrt{D_1}}{(\gamma-1)} & \text{for } \gamma < 1 \text{ or } \gamma > 1 \end{cases}$ $D_1 = (B_s + B_f + 1 + (1/\beta)F_{pr})^2 - (1-\gamma)(1+2B_s(1-\Delta_s) + 2B_f(1-\Delta_f) + (2/\beta)F_{pr})$
2.1.1.1	$k_{2111} = \dfrac{D_{2111} + \beta^2(B_s+B_f) + \beta F_{pr} - \sqrt{\left[(D_{2111} + \beta^2(B_s+B_f) + \beta F_{pr})^2 - (D_{2111} - \beta^2\gamma)(D_{2111} + 2\beta^2(B_s(1-\Delta_s) + B_f(1-\Delta_f)) + 2\beta F_{pr})\right]}}{D_{2111} - \beta^2\gamma}$ $D_{2111} = \eta(\beta-1)^2 + 2\beta - 1$
2.1.2.1	$k_{2121} = \dfrac{D_{2121} + \zeta\beta B_s + \beta^2 B_f + \beta F_f^{pr} - \sqrt{(D_{2121} + \zeta\beta B_s + \beta^2 B_f + \beta F_f^{pr})^2 - (D_{2121} - \beta^2\gamma)(D_{2121} + 2\zeta\beta B_s + 2\beta^2 B_f(1-\Delta_f) + 2\beta F_f^{pr})}}{D_{2121} - \beta^2\gamma}$ $D_{2121} = \eta(\beta-1)^2 + 2\beta - 1$
2.2.1.1	$k_{2211} = \dfrac{D_{2211} + \omega\gamma\beta + \beta^2(B_s+B_f) + \beta F_{pr} - \sqrt{\left[(D_{2211} + \omega\gamma\beta + \beta^2(B_s+B_f) + \beta F_{pr})^2 - (D_{2211} + 2\omega\gamma\beta)(D_{2211} + 2\beta^2 B_s(1-\Delta_s) + 2\beta^2 B_f(1-\Delta_f) + 2\beta F_{pr})\right]}}{D_{2211} + 2\omega\gamma\beta}$ $D_{2211} = \eta(\beta-1)^2 + 2\beta - 1 + \omega^2\gamma$
2.2.2.1	$k_{2221} = \dfrac{D_{2221} + \beta(\zeta B_s + \omega\gamma + F_f^{pr}) + \beta^2 B_f - \sqrt{(D_{2221} + \beta(\zeta B_s + \omega\gamma + F_f^{pr}))^2 - (D_{2221} + 2\omega\gamma\beta)(D_{2221} + 2\beta(\zeta B_s + 2\beta F_f^{pr}) + 2\beta^2 B_f(1-\Delta_f))}}{D_{2221} + 2\omega\gamma\beta}$ $D_{2221} = \eta(\beta-1)^2 + 2\beta - 1 + \omega^2\gamma$
3.1.1.1	$k_{3111} = \dfrac{D_{3111} + \beta^2(B_s+B_f) + \beta F_{pr} - \sqrt{(D_{3111} + \beta^2(B_s+B_f) + \beta F_{pr})^2 - (D_{3111} - \beta^2\gamma)(D_{3111} + 2\beta^2(B_s(1-\Delta_s) + B_f(1-\Delta_f)) + 2\beta F_{pr})}}{D_{3111} - \beta^2\gamma}$ $D_{3111} = \eta(\alpha-1)^2 + 2(\alpha(1-\mu) + \mu\beta) - 1$
3.1.2.1	$k_{3121} = \dfrac{D_{3121} + \beta(\zeta B_s + F_f^{pr}) + \beta^2 B_f - \sqrt{(D_{3121} + \beta(\zeta B_s + F_f^{pr}) + \beta^2 B_f)^2 - (D_{3121} - \beta^2\gamma)(D_{3121} + 2\beta\zeta B_s + 2\beta^2 B_f(1-\Delta_f) + 2\beta F_f^{pr})}}{D_{3121} - \beta^2\gamma}$ $D_{3121} = \eta(\alpha-1)^2 + 2(\alpha(1-\mu) + \mu\beta) - 1$
3.2.1.1	$k_{3211} = \dfrac{D_{3211} + \beta^2(B_s+B_f) + \beta(\omega\gamma + F_{pr}) - \sqrt{\left[D_{3211} + \beta^2(B_s+B_f) + \beta(\omega\gamma + F_{pr})^2 - (D_{3211} + 2\omega\gamma\beta)(D_{3211} + 2\beta^2(B_s(1-\Delta_s) + B_f(1-\Delta_f)) + 2\beta F_{pr})\right]}}{D_{3211} + 2\omega\gamma\beta}$ $D_{3211} = \eta(\alpha-1)^2 + 2(\alpha(1-\mu) + \mu\beta) + \omega^2\gamma - 1$
3.2.2.1	$k_{3221} = \dfrac{D_{3221} + \beta(\zeta B_s + \omega\gamma + F_f^{pr}) + \beta^2 B_f - \sqrt{\left[(D_{3221} + \beta(\zeta B_s + \omega\gamma + F_f^{pr}) + \beta^2 B_f)^2 - (D_{3221} + 2\omega\gamma\beta)(D_{3221} + 2\zeta\beta B_s + 2\beta^2 B_f(1-\Delta_f) + 2\beta F_f^{pr})\right]}}{D_{3221} + 2\omega\gamma\beta}$ $D_{3221} = \eta(\alpha-1)^2 + 2(\alpha(1-\mu) + \mu\beta) + \omega^2\gamma - 1$

$B_s = \gamma_s \rho_s (1-\Delta_s)$, $B_f = \gamma_f \rho_f (1-\Delta_f)$, $F_{pr} = F_s^{pr} + F_f^{pr}$

By applying the Virtual Work Method, the mid-span deflection of the beam for the ith loading step, $(\delta_{mid})_i$, is determined, as well as its corresponding force P_i that constitute a point of the $P-\delta$ curve.

Table 2 - Equations for the evaluation of the normalized moment, M', and normalized curvature, χ', for stage i [11].

i	M'
1	$M_1' = \dfrac{2\beta\left[(\gamma-1)k_1^3 + 3(B_s+B_f+1)k_1^2 + 3\left(2B_s(1-\Delta_s)+2B_f(1-\Delta_f)-1\right)k_1 + 3\left(B_s(\Delta_s-1)^2+B_f(\Delta_f-1)^2\right)+1\right]}{(1-k_1)} + \left(M_{pr}'\right)_1$ $\left(M_{pr}'\right)_1 = 6F_s^{pr}(1-k_1-\Delta_s) + 6F_f^{pr}(1-k_1-\Delta_f)$
2.1.1.1	$M_{2111}' = \dfrac{(2\beta\gamma+C_{2111})k_{2111}^3 + 3(2\beta B_s+2\beta B_f-C_{2111})k_{2111}^2 + 3\left(C_{2111}-4\beta(B_s(1-\Delta_s)+B_f(1-\Delta_f))\right)k_{2111}+6\beta B_s(1-\Delta_s)^2+6\beta B_f(1-\Delta_f)^2-C_{2111}}{(1-k_{2111})} + \left(M_{pr}'\right)_{2111}$ $C_{2111} = \dfrac{-2\eta\beta^3+3\eta\beta^2-3\beta^2-\eta+1}{\beta^2}$, $\left(M_{pr}'\right)_{2111} = 6F_s^{pr}(1-k_{2111}-\Delta_s)+6F_f^{pr}(1-k_{2111}-\Delta_f)$
2.1.2.1	$M_{2121}' = \dfrac{(2\beta\gamma+C_{2121})k_{2121}^3 + 3(2\zeta B_s+2\beta B_f-C_{2121})k_{2121}^2 + 3\left(C_{2121}+2\zeta B_s(\Delta_s-2)-4\beta B_f(1-\Delta_f)\right)k_{2121}+6\zeta B_s(1-\Delta_s)+6\beta B_f(1-\Delta_f)^2-C_{2121}}{(1-k_{2121})} + \left(M_{pr}'\right)_{2121}$ $C_{2121} = \dfrac{-2\eta\beta^3+3\eta\beta^2-3\beta^2-\eta+1}{\beta^2}$, $\left(M_{pr}'\right)_{2121} = 6F_f^{pr}(1-k_{2121}-\Delta_f)$
2.2.1.1	$M_{2211}' = \dfrac{-(3\omega\gamma+C_{2211})k_{2211}^3 + 3(\omega\gamma+C_{2211}+2\beta B_s+2\beta B_f)k_{2211}^2 - 3\left(4\beta(B_s(1-\Delta_s)+B_f(1-\Delta_f))+C_{2211}\right)k_{2211}-6\beta B_s(1-\Delta_s)^2-6\beta B_f(1-\Delta_f)^2+C_{2211}}{(1-k_{2211})}$ $\qquad\qquad\qquad + \left(M_{pr}'\right)_{2211}$ $C_{2211} = \dfrac{2\eta\beta^3-3\eta\beta^2+3\beta^2-\omega^3\gamma+\eta-1}{\beta^2}$, $\left(M_{pr}'\right)_{2211} = 6F_s^{pr}(1-k_{2211}-\Delta_s)+6F_f^{pr}(1-k_{2211}-\Delta_f)$
2.2.2.1	$M_{2221}' = \dfrac{-(3\omega\gamma+C_{2221})k_{2221}^3 + (3\omega\gamma+3C_{2221}+6\zeta B_s+6\beta B_f)k_{2221}^2 - \left((12\zeta B_s-6\zeta B_s\Delta_s)+3C_{2221}-12\beta B_f(1-\Delta_f)\right)k_{2221}+6\zeta B_s\Delta_s+6\beta B_f(1-\Delta_f)^2+C_{2221}}{(1-k_{2221})} + \left(M_{pr}'\right)_{2221}$ $C_{2221} = \dfrac{2\eta\beta^3-3\eta\beta^2+3\beta^2-\omega^3\gamma+\eta-1}{\beta^2}$, $\left(M_{pr}'\right)_{2221} = 6F_f^{pr}(1-k_{2221}-\Delta_f)$
3.1.1.1	$M_{3111}' = \dfrac{(C_{3111}-2\beta\gamma)k_{3111}^3 - 3(2\beta B_s+2\beta B_f+C_{3111})k_{3111}^2 + 3\left(C_{3111}+4\beta(B_s(1-\Delta_s)+B_f(1-\Delta_f))\right)k_{3111}-6\beta\left(B_s(1-\Delta_s)^2+B_f(1-\Delta_f)^2\right)-C_{3111}}{(k_{3111}-1)} + \left(M_{pr}'\right)_{3111}$ $C_{3111} = \dfrac{3\left(\mu\beta^2-\mu\alpha^2-\eta\alpha^2+\alpha^2\right)+2\eta\alpha^3+\eta-1}{\beta^2}$, $\left(M_{pr}'\right)_{3111} = 6F_s^{pr}(1-k_{3111}-\Delta_s)+6F_f^{pr}(1-k_{3111}-\Delta_f)$
3.1.2.1	$M_{3121}' = \dfrac{(C_{3121}-2\beta\gamma)k_{3121}^3 - 3(2\zeta B_s+2\beta B_f+C_{3121})k_{3121}^2 + 3\left(C_{3121}+2\zeta B_s(2-\Delta_s)+4\beta B_f(1-\Delta_f)\right)k_{3121}-6\left(\zeta B_s(1-\Delta_s)+\beta B_f(1-\Delta_f)^2\right)-C_{3121}}{(k_{3121}-1)} + \left(M_{pr}'\right)_{3121}$ $C_{3121} = \dfrac{3\left(\mu\beta^2-\mu\alpha^2-\eta\alpha^2+\alpha^2\right)+2\eta\alpha^3+\eta-1}{\beta^2}$, $\left(M_{pr}'\right)_{3121} = 6F_f^{pr}(1-k_{3121}-\Delta_f)$
3.2.1.1	$M_{3211}' = \dfrac{-(3\omega\gamma+C_{3211})k_{3211}^3 + 3(\omega\gamma+C_{3211}+2\beta(B_s+B_f))k_{3211}^2 - 3\left(4\beta(B_s(1-\Delta_s)+\beta B_f(1-\Delta_f))+C_{3211}\right)k_{3211}+6\beta\left(B_s(1-\Delta_s)^2+B_f(1-\Delta_f)^2\right)+C_{3211}}{(1-k_{3211})}$ $\qquad\qquad\qquad + \left(M_{pr}'\right)_{3211}$ $C_{3211} = \dfrac{3\left(\mu\beta^2-\mu\alpha^2-\eta\alpha^2+\alpha^2\right)+2\eta\alpha^3-\omega^3\gamma+\eta-1}{\beta^2}$, $\left(M_{pr}'\right)_{3211} = 6F_s^{pr}(1-k_{3211}-\Delta_s)+6F_f^{pr}(1-k_{3211}-\Delta_f)$
3.2.2.1	$M_{3221}' = \dfrac{-(3\omega\gamma+C_{3221})k_{3221}^3 + (3\omega\gamma+3C_{3221}+6(\zeta B_s+\beta B_f))k_{3221}^2 - 3\left(2\zeta B_s(2-\Delta_s)+4\beta B_f+C_{3221}\right)k_{3221}+6\zeta B_s(1-\Delta_s)+6\beta B_f(1-\Delta_f)^2+C_{3221}}{(1-k_{3221})} + \left(M_{pr}'\right)_{3221}$ $C_{322} = \dfrac{3\left(\mu\beta^2-\mu\alpha^2-\eta\alpha^2+\alpha^2\right)+2\eta\alpha^3-\omega^3\gamma+\eta-1}{\beta^2}$, $\left(M_{pr}'\right)_{3221} = 6F_f^{pr}(1-k_{3221}-\Delta_f)$

$B_s = \gamma_s\rho_s(1-\Delta_s)$, $B_f = \gamma_f\rho_f(1-\Delta_f)$, $F_{pr} = F_s^{pr}+F_f^{pr}$, $\chi_i' = 0.5\beta/(1-k_i)$
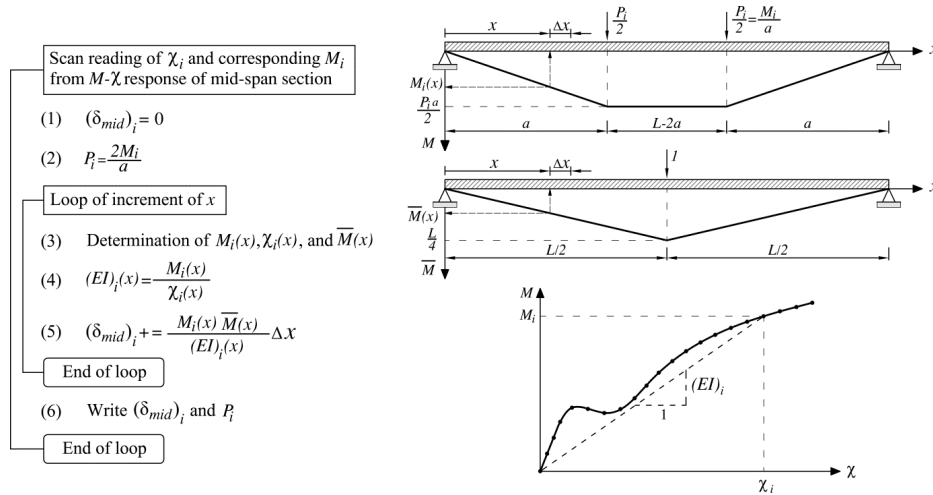
Figure 3: Numerical approach to simulate the force-deflection response of simple supported beams failing in bending

3 Model assessment

The load carrying capacity predicted by the proposed model for a simply supported hybrid reinforced FRC beam (Fig. 4) was evaluated by performing a material nonlinear analysis with the FEMIX computer code [9]. For this simulation the smeared crack model described in detail elsewhere [12] was used.
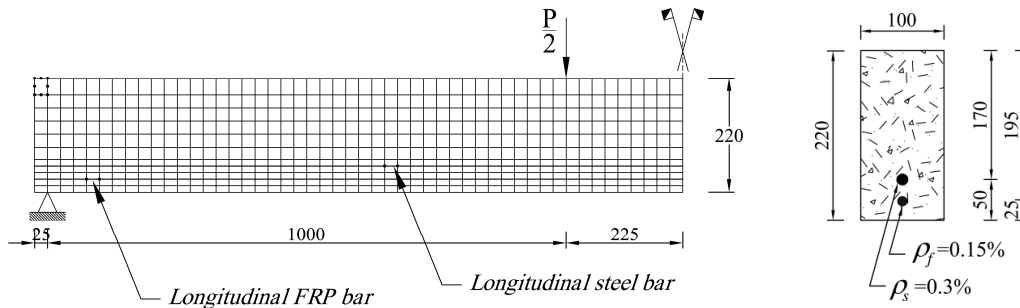

Figure 4: Geometry, reinforcement data, and mesh details of the beam used in model assessment and parametric study (dimensions in mm).

In Fig. 4 is also depicted the finite element mesh adopted, where FRC was simulated by using Plane Stress 2D elements, while Truss 2D elements were considered for both FRP and steel bars. Table 3 includes the values that characterize the intervening materials, in which two distinct values were utilized for the α and μ parameters, and for pre-stress levels ($\varepsilon_f^{pr}/\varepsilon_{fu}$ and $\varepsilon_s^{pr}/\varepsilon_{sy}$ for steel and FRP bars, respectively).

Table 3: Values for the parameters properties adopted in the model assessment

ε_{cr} (‰)	E (GPa)	α	μ	β_{tu}	ω	γ	λ_{cu}	ζ	γ_s	$\varepsilon_s^{pr}/\varepsilon_{sy}$	ψ_{su}	ν_{fu}	γ_f	$\varepsilon_f^{pr}/\varepsilon_{fu}$
0.1	35	50 100	0.4 0.8	150	20	1	35	75	5.71	0.25 0.50	150	166.7	1.71	0.25 0.50

8
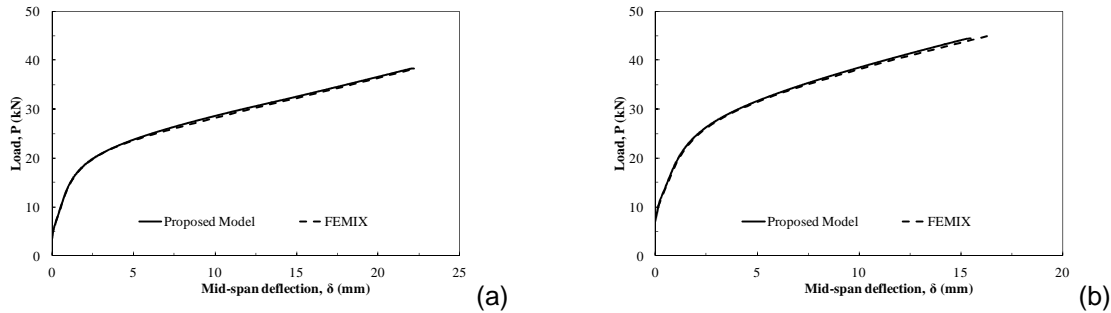
Figure 5: Load-Deflection responses predicted by the model and FEMIX software for: (a) $\alpha = 50$, $\mu = 0.4$ and Pr=25%; (b) $\alpha = 100$, $\mu = 0.8$ and Pr=50%.

In Fig. 5 the results of the model are compared with those obtained from FEMIX, where it is visible that the closed-formulation is capable of predicting with high accuracy the deformational response of this type of structural elements.

4 Parametric study

To assess the influence of the relevant mechanical properties of FRC, and the pre-stressed level applied to FRP and steel bars, on the moment-curvature relationship and on the force-deflection of the adopted hybrid reinforcement, a parametric study was carried out on a beam type with the geometry, the reinforcement arrangement and the loading conditions represented in Fig. 4. Three distinct pre-stress levels were considered, 0% (non pre-stressed), 25%, and 50%. For the influence of the FRC post-cracking performance, the values of 1.01, 10, 50, and 150 for the normalized transition strain (α) were adopted, maintaining constant the normalized residual strength of $\mu = 0.6$. The values of the parameters that define the constitutive laws of the intervening materials in the performed parametric study are indicated in Table 4.

Table 4 : Values for the parameters of the materials adopted in the parametric study

Concrete (tension)					Concrete (compression)			Steel bar			FRP bar	
ε_{cr} (‰)	E (GPa)	α	μ	β_{tu}	ω	γ	λ_{cu}	ζ	γ_s	ψ_{su}	ν_{fu}	γ_f
0.1	35	[1.01, 10, 50, 150]	0.6	150	20	1	35	75	5.71	150	166.7	1.71

The results of the parametric study are presented in Figs. 6 and 7, where the points corresponding to the concrete crack initiation and the steel yield initiation are signalized in the moment-curvature and in the force-deflection curves. As expected, for the considered statically determinate beam the variation of load-deflection follows the variation of the corresponding moment-curvature. For each adopted pre-stress level of FRP and steel bars, the influence of α FRC-related parameter in terms of moment-curvature and load-deflection responses is represented in Figures 6a-c and 6d-f, respectively. Since α is a post cracking parameter of FRC, it has no effect in the responses before crack initiation. However, after crack initiation the flexural capacity of the cross section and the load carrying capacity of the beam are significantly increased with the increase of α parameter. In fact, the moment and the load at yield initiation of steel bars increase with α, and this tendency is also observed for the corresponding curvatures and deflections.
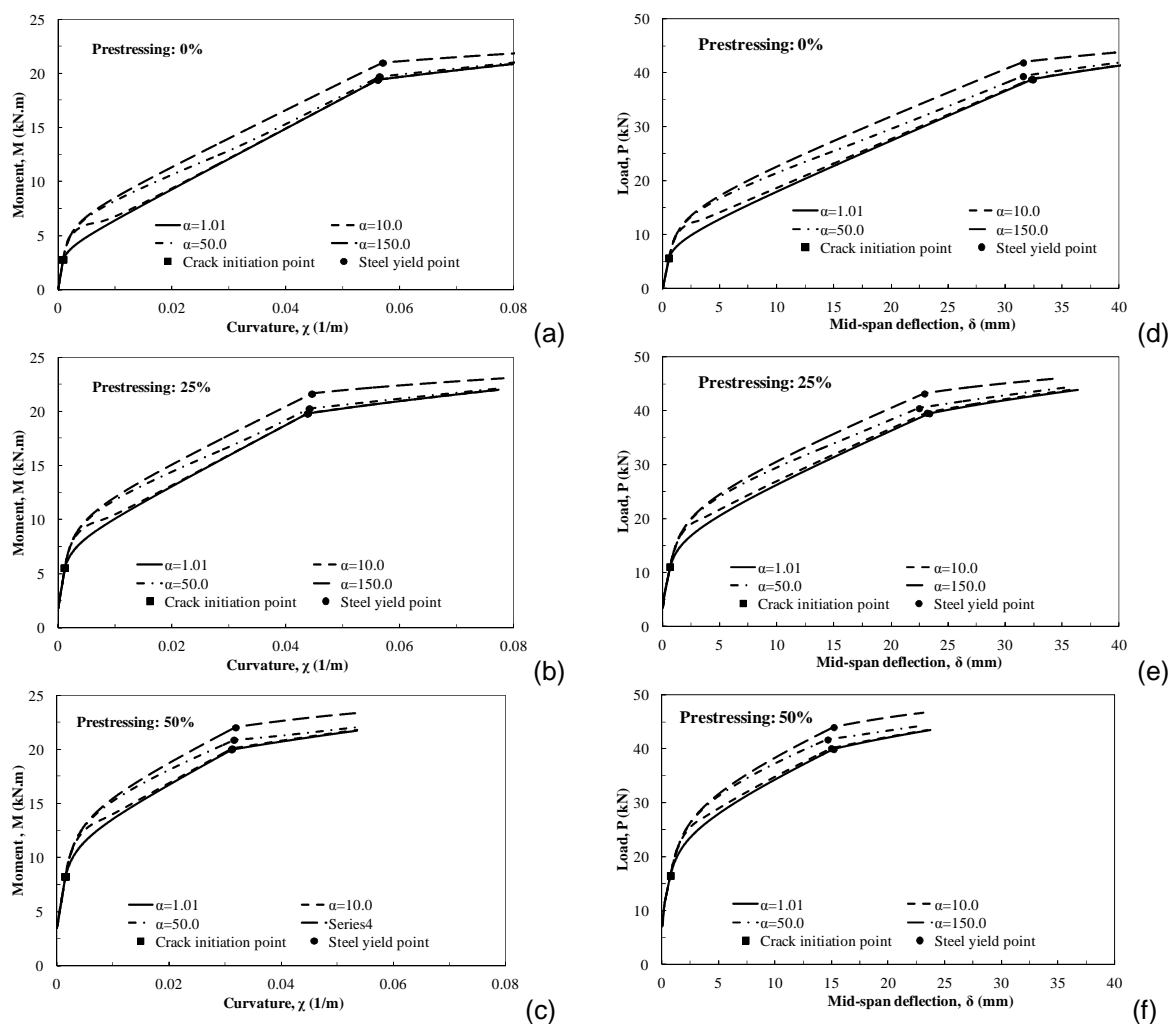
9

Figure 6: Effect of the α parameter on the moment-curvature and load-deflection responses for $\mu = 0.6$, and steel and FRP bars pre-stressed at: (a) 0.0, (b) 25, and (c) 50%.

The influence of the pre-stress percentage on the moment-curvature and load-deflection responses is illustrated in Figure 7a-d and 7e-h, respectively, for the different values of α considered. As expected, for a given α value, the moment and the load at crack initiation have increased with the applied pre-stress, but the moment and the load at yield initiation of the steel bars was not significantly affected by the pre-stress level. However, due to the initial tensile strain introduced in the steel bars when pre-stress is applied, the curvature and the deflection at yield initiation decrease with the increase of the pre-stress level, being this effect as pronounced as high is the pre-stress level.

5 CONCLUSIONS

In this work a design oriented model was proposed for the determination of the moment-curvature and the load deflection response of rectangular cross section of FRC members failing in bending, and reinforced with longitudinal pre-stressed steel and FRP bars. By using a trilinear stress-strain diagram for the tensile behaviour of FRC, the proposed model is capable of simulating both strain softening and strain hardening FRC materials.
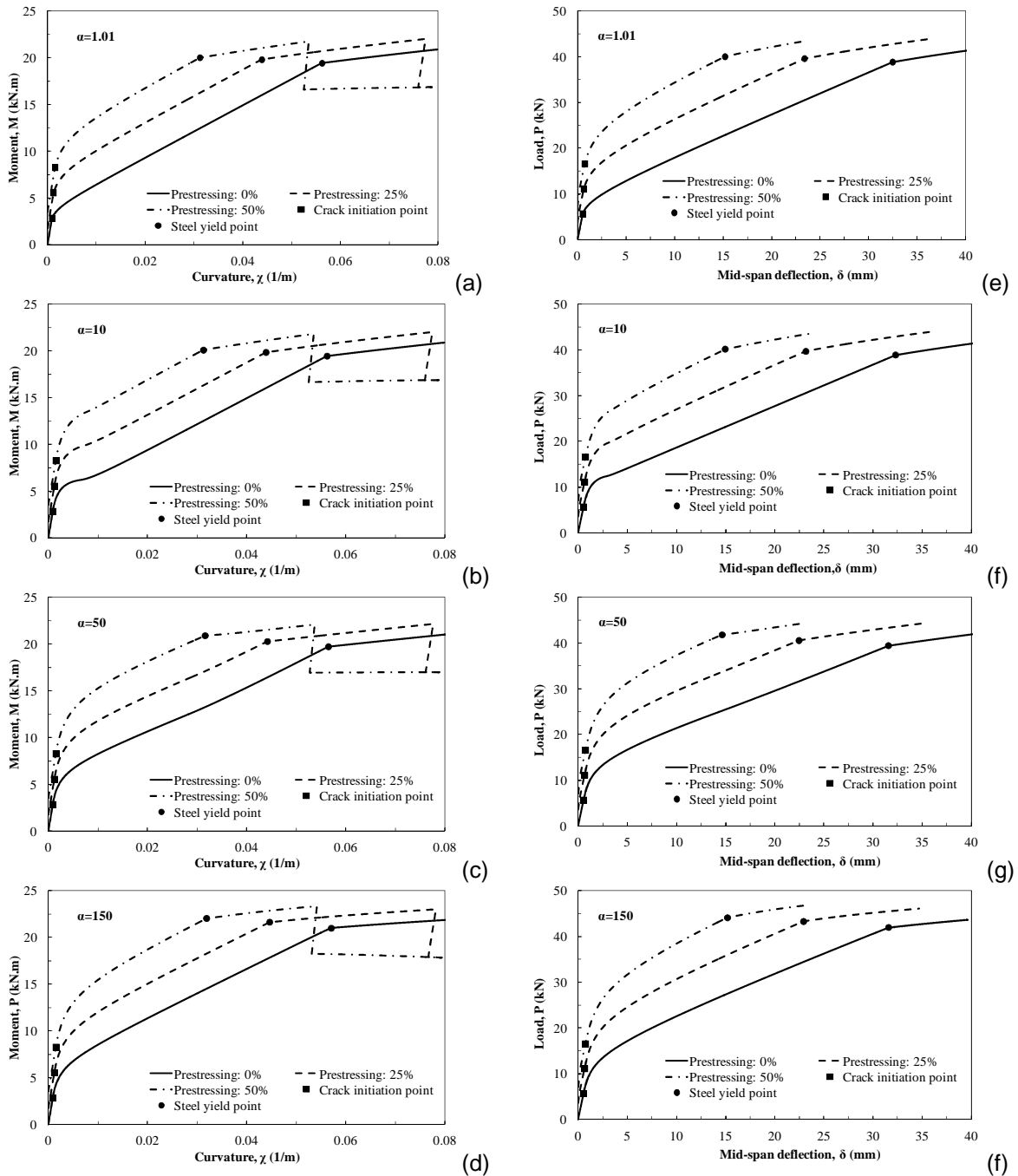
Figure 7: Effect of the pre-stress level on the: (a-d) moment-curvature response; (e-h) load-deflection response; for $\mu = 0.6$ and α equal to 1.01, 10.0, 50.0 and 150.0.

The good predictive performance of the model was assessed by using the FEM-based FEMIX software. The parametric studies executed by using the proposed model have revealed that the flexural capacity and the load carrying capacity of the beam are significantly increased with the increase of the α parameter, which defines the continuous decrease of residual strength of a FRC

just after the crack initiation phase. Furthermore, by increasing the pre-stress level to the steel and FRP bars, the curvature and the deflection at steel yield initiation, as well as the curvature and the deflection at failure have decreased. Therefore, since the deflection at crack initiation is not affected significantly by the pre-stress level applied, the deflection amplitude between crack initiation and steel yield initiation has decreased with the increase of the pre-stress level, reducing the ductility of the response of the beams. However, the FRC can be optimized in order to provide values for the α parameters that guarantee the aimed degree of ductility when applying a certain pre-stress level in a hybrid reinforced beam.

ACKNOWLEDGEMENTS

REFERENCES

[1] M. Thériault and B. Benmokrane, "Effects of FRP Reinforcement Ratio and Concrete Strength on Flexural Behaviour of Concrete Beams", J. Composites for Construction, 2(1), 7-16 (1998).

[2] Y. Tian and Y. Yuan, "Deflection Prediction of Concrete Beams Reinforced with GFRP and Steel Rods", Proceedings (CD-ROM) of 8th International Symposium on Fibre Reinforced Polymer (FRP) Reinforcement for Concrete Structures (FRPRCS-8), Patras, 16-18 (2007).

[3] ACI 440R-07. "Report on Fibre-Reinforced Polymer (FRP) Reinforcement for Concrete Structures", American Concrete Institute Reported by ACI Committee 440 2007: 100 pages.

[4] CEB-FIP. "FRP reinforcement in RC structures". Technical report on the Design and use of fibre reinforced polymer reinforcement (FRP) in reinforced concrete structures, prepared by a working party of the Task Group 9.3 2007: 175 pages.

[5] M.A. Aiello and L. Ombres, "Structural Performances of Concrete Beams with Hybrid (Fibre-Reinforced Polymer-Steel) Reinforcements", J. Composites for Construction 6(2), 133-140 (2002).

[6] H. Nordin and B. Taljsten, "Concrete beams strengthened with pre-stressed near surface mounted CFRP", J. Composites for Construction, 10(1), 60-68 (2006).

[7] P.F.S. Santos, J.A.O. Barros, L.A.P. Lourenço, "Steel fibres for the shear resistance of high strength concrete beams", Proceedings of 7th RILEM International Symposium on Fibre Reinforced Concrete Design and Applications (BEFIB 2008), Paper SIM01, Chennai, India, 17-19 (2008).

[8] A. Naaman, "High performance fibre reinforced cement composites", In C. Shi, & Y. Mo, "High-performance construction materials (Science and Application)". World Scientific Publishing Co. Pte. Ltd. (2008).

[9] A.F.M. Azevedo, J.A.O. Barros, J.M. Sena-Cruz, and A.V. Gouveia, "Software no ensino e no projecto de estruturas. Educational software for the design of structures." Proceedings of III Congresso de Luso-Moçambicano de Engenharia, J.S. Gomes, C.F. Afonso, C.C. António and A.S. Matos (eds.), Maputo, Mozambique, 81-92 [in Portuguese] (2003).

[10] C. Soranakom and B. Mobasher, "Correlation of tensile and flexural response of strain softening and strain hardening cement composites". Cement & Concrete Composites, 30, 465-477 (2008).

[11] M. Taheri, J.A.O. Barros and H. Salehian, "A design model for fibre reinforced concrete elements reinforced by longitudinal pre-stressed steel and FRP bars failing in bending", Technical report 11-DEC/E-18, Department of Civil Engineering, University of Minho, pp. 59, (2011).

[12] A. Ventura-Gouveia,J.A.O Barros, A.F.M. Azevedo, "Crack constitutive model for the prediction of punching failure modes of fiber reinforced concrete laminar structures", Computers & Concrete, 8(6), 735-755 (2011).